Phonon scattering: how does it affect the image contrast in high-resolution transmission electron microscopy?

Z. L. WANG[†]

School of Materials Science and Engineering, Georgia Institute of Technology, Atlanta, Georgia 30332-0245, USA

ABSTRACT

In quantitative high-resolution transmission electron microscopy (HRTEM), the theoretically calculated images usually give better contrast than the experimentally observed images although all the factors have been accounted for. It is suggested that this discrepancy is due to thermal diffusely scattered electrons, which were not included in the image calculation. The question is: how do they affect the image contrast? In this paper, under the weak-phase object approximation, it is shown that the contribution of the thermal diffusely scattered electrons to the image is of the same order as the cross-interference terms for the Bragg reflected beams in the dark-field HRTEM imaging. Indirect experimental measurements showed that thermal diffuse scattering (TDS) is not a small effect; rather it is the dominant scattering at large angles. The TDS absorption is measured and the result indicates that about 12% of the incident electrons have been diffusely scattered to angles larger than $15.6°$ (the column angle of the transmission electron microscope) by a Si foil as thin as 15–20 nm. The data clearly show the magnitude and importance of TDS in HRTEM. It is therefore mandatory to include this component in image calculation.

§1. INTRODUCTION

Instrumentation development in recent years has made it possible to perform quantitative high-resolution transmission electron microscopy (HRTEM), in which the simulated images are refined with reference to the experimentally observed images to determine the crystal structure. Three key factors are indispensable for quantitative HRTEM: an energy-filtering system that can remove all the inelastically scattered electrons except phonon-scattered electrons, a high-quality charge-coupled device (CCD) camera which has single-electron sensitivity for digital data recording, and a precise dynamic diffraction theory and adequate calculation techniques for quantifying the data. Removing of the inelastically scattered electrons with energy losses larger than a few electronvolts quite significantly simplifies the data analysis, but the removed electrons are effectively equivalent to an absorption effect on the elastically scattered electrons. On the other hand, some of the phonon-scattered electrons still remain in the image; one needs to find out how this process affects the image contrast and how large this effect is. These are the questions that we try to answer in this paper. In practice, the calculated image based on the multislice theory for elastic scattering gives better contrast than the experimentally observed image although considerations have been made accounting for the effects of the beam

---

† Email: zhong.wang@mse.gatech.edu.

convergence, the energy spread of the source, the mechanical vibration of the micro-scope, the Debye–Waller factor, the absorption function, the surface amorphous layer, the lens instability, the digital data recording, the electron energy filtering, etc. (Van Dyck 1997). The only thing excluded is the thermal diffusely scattered electrons, because they are rather difficult to introduce into a multislice calculation.

In this paper, we first present the physical argument of why phonon-scattered electrons are important for quantifying image contrast. Then, the contribution of phonon-scattered electrons to HRTEM images is investigated using the weak-phase object approximation to explore the physical nature. Finally, some experimental results are shown to support the theoretical conclusion.

§2. Why phonon-scattered electrons?

Inelastic interaction of an incident electron with the crystal can be classified into two categories (Wang 1995a): quantum transitions and continuous energy-losses. There are three basic processes in the class of quantum transitions. First, plasmon (or valence) excitation characterizes the transitions of electrons from the valence band to the conduction band. The energy-loss for a single-plasmon excitation is in the range 1–40 eV, and multiple-plasmon excitation is enhanced if specimens are thick. The momentum transfer introduced in plasmon excitation is usually small; thus, the typical angular spreading to the diffracted beam is less than 0.2 mrad for a single-loss event. The plasmon excitation is a collective excitation of the crystal electrons and the localization of the excitation is rather large; thus, the uniform excitation of the plasmon loss electrons in the specimen does not affect the elastic scattering behaviour of the electrons, although the subsequent diffraction of the plasmon-loss electrons can still give lattice images. The effect of the plasmon loss on the elastic wave can be represented by a constant absorption factor $\exp(-d/\Lambda)$, where d is the specimen thickness and Λ is the inelastic mean-free-path length, equivalent to a reduction in overall intensity. The image formed by the plasmon-loss electrons can be totally removed by the energy filter. Therefore, one does not need to consider plasmon excitation in HRTEM image calculation if the specimen thickness is uniform.

Secondly, atomic inner-shell ionization can be excited and it usually produces a significant amount of energy loss, but the question is: how significant is this process? With the use of the SIGMAL program based on the hydrogen-like model (Egerton 1996), the integrated ionization cross-section of the Si L edge with an energy window of 100 eV, for example, is calculated to be $\sigma_L = 8.49 \times 10^{-20}$ cm^2 for 200 kV elec-trons. For a thin Si foil of 25 nm thickness, the probability that an incident electron excites the Si L edge can be calculated from

$$P = \sigma_L nd, \tag{1}$$

where n is the density of atoms in the specimen and d is the specimen thickness, which yields about 0.94% for the Si L edge and 0.004% for the Si K edge. This is extraordinary small, even smaller than the inaccuracy of the experiments. Therefore, atomic inner-shell excitation can be ignored in the image calculation, although this is a localized scattering process.

Finally, thermal diffuse scattering (TDS) or phonon scattering is the result of atomic vibrations in crystals. This process does not introduce any significant energy loss but produces large momentum transfer, which can scatter the incident electron out of the selected angular range of the objective aperture. Thermal vibrations of

crystal atoms perturb the potential function of the crystal; thus, the scattering behaviour of the incident electron is perturbed. This is the electro–phonon interaction process. To incorporate thermal vibrations properly in the calculation, an average crystal potential V_0 is introduced, which is defined to be the time average of the crystal potential and it is a periodic, time-independent function. The instantaneous crystal potential is written as a sum of the average potential V_0 and a time-dependent perturbation component ΔV

$$V(\mathbf{r}, t) = V_0(\mathbf{r}) + \Delta V(\mathbf{r}, t). \qquad (2)$$

V_0 is responsible for the Bragg reflections and ΔV for the diffuse scattering. The first question is how important is ΔV? To answer this question, figure 1 shows the calculated instantaneous potential V, the thermal equilibrium potential V_0 and the
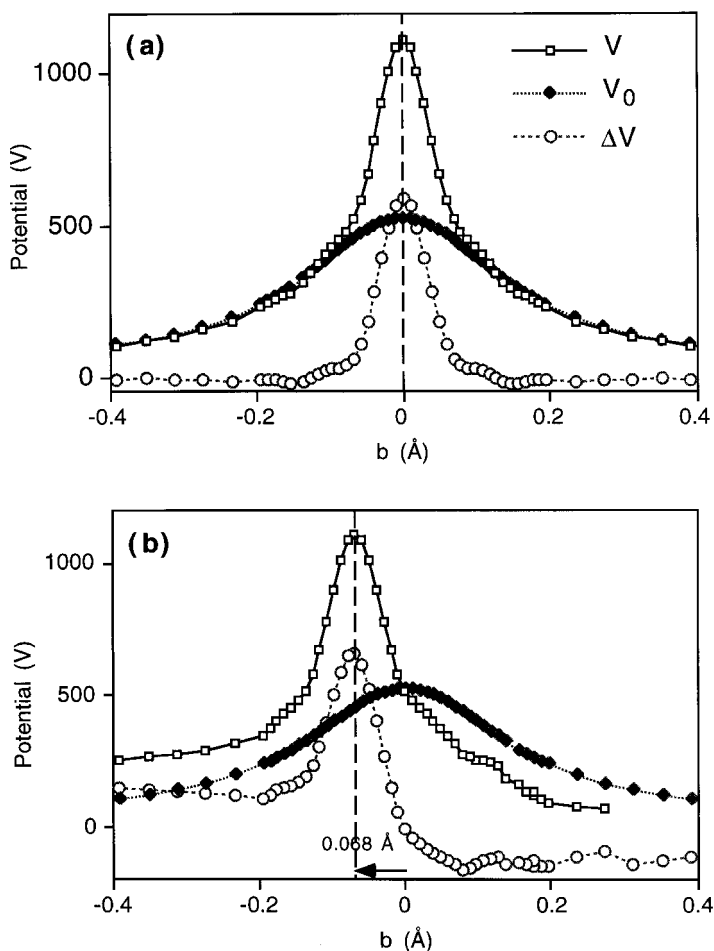
Figure 1. Potential of a silicon atom with (V_0) and without (V) the Debye–Waller factor. V is the instantaneous atomic potential and V_0 is the time-averaged atomic potential. The equilibrium position of the atom is $b = 0$. $\Delta V = V - V_0$ (- - - - -) is the deviation of the atomic potential from the time-averaged potential V_0 when the atomic displacement is (a) $a_\kappa = 0\,\text{Å}$ or (b) $a_\kappa = -0.068\,\text{Å}$. The arrow in (b) indicates the displacement of the atom. The rms atom vibration amplitude was taken as $0.07\,\text{Å}$ in the calculation.

difference $\Delta V = V - V_0$ for a Si atom using the experimentally determined rms vibration amplitude of Si. If the instantaneous position of the atom is its equilibrium lattice site, ΔV is a symmetric sharp function. If the atom is displaced to an instantaneous position located at 0.068 Å on the left-hand side from the equilibrium site, ΔV is no longer symmetric (figure 2(b)). Two striking characteristics are noticed. One is that the magnitude of ΔV is compatible with that of V_0 and this is true for each atom present in the specimen. The other is that ΔV is considerably narrower than V_0, indicating that TDS is a rather localized scattering process, with the majority of the electrons being generated from the nuclear sites, indicating that a higher resolution could be achieved using phonon-scattered electrons (Cowley 1988). On the other hand, the mean-free-path lengths of TDS at 200 kV are 1000 nm for Si and 180 nm for GaAs at 300 K (Rossouw *et al.* 1990); thus, the probability that an incident electron is scattered by phonons is of the order of 2.5% for Si and 13.4% in GaAs for a thin foil of 25 nm thickness. *This percentage is small but this small amount of electrons come from the nuclear sites. Therefore, the image contrast is likely to be affected by TDS.* In contrast with atomic inner-shell excitation, whose probability has no strong dependence on atomic number, the probability of phonon scattering increases dramatically as the atomic number increases because of the stronger scattering power.

The localization of phonon excitation can be seen in the calculated single-atom scattering factors for elastic scattering and TDS (figure 2). It is apparent that the small-angle scattering is dominated by elastic scattering, while the large-angle scattering is dominated by TDS. This dominant effect is apparent when the scattering angle is larger than the Bragg angle of (880). At the first-order Laue zone (FOLZ) position, TDS is about six times stronger than the elastic scattering. In real space,
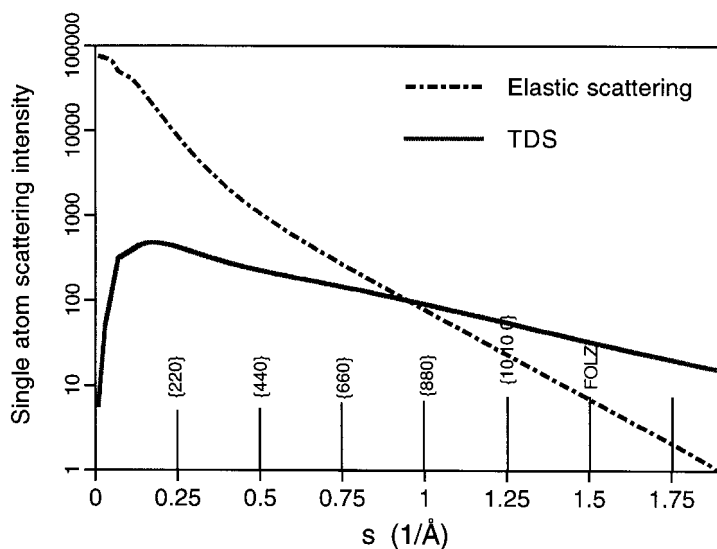
Figure 2. Theoretically calculated atom scattering factor $[(f^e)^2 \exp(-2W)]$ for elastic scattering and atom scattering factor $(f^e)^2[1 - \exp(-2W)]$ for the TDS of a Si atom, showing the dominant contribution of TDS at large scattering angles, where W is the Debye–Waller factor. The scattering vector $\mathbf{s} = \mathbf{g}/2$. The rms atomic vibration amplitude was taken as 0.07 Å in the calculation.

TDS is expected to be more localized than the elastic scattering; thus, the image intensity at the centres of atomic columns is likely to be affected by TDS. As today's image resolution approaches 1 Å (Coene *et al.* 1994, Dehm *et al.* 1996, Van Dyck *et al.* 1997), the sharp peaks of atomic columns can be revealed experimentally; thus, the effect of TDS could be enhanced with the improvement of image resolution. It is thus mandatory to include it in image simulation.

The continuous energy-loss processes include bremsstrahlung radiation, produced in the collision of the incident electron with crystal atoms, and electron Compton scattering, produced in the collision of the incident electron with a crystal electron. Both processes are not completely delocalized but the localization is much larger than the size of the atomic potential. On consideration of the wide range of continuous energy losses, they are unlikely to affect the image contrast in the atomic dimension but contribute a background. This background can be removed with the use of an energy filter.

§3. How do the phonon-scattered electrons affect the image contrast?

We have illustrated the physical background on the basis of which the phonon scattered electrons is likely to affect the image contrast. The question now is: how do these electrons affect the image contrast? To answer this question, one uses the 'frozen' lattice model (Hall and Hirsch 1965), which means that, although atom vibration is a time-dependent process, the crystal lattice appears as if in a stationary instantaneous configuration for an incident electron since the interaction time of the electron with the crystal is much shorter than the vibration period of the crystal atom, but the crystal lattice can be in another configuration for the next incoming electron. Thus, for each lattice configuration, the scattering of the electron can be considered as a time-independent quasi-elastic scattering process, and the final observed diffraction pattern or image is equivalent to a time average on the intensities calculated for the different lattice configurations. To simplify our discussion, the weak-phase object approximation is used although it is believed to be a unrealistic approximation but it is still the best model for illustrating the physics involved in the image formation. Hence, the electron wave after exiting the crystal surface can be represented by

$$\Phi(\mathbf{b}) \approx 1 + i\sigma V_{\mathrm{p}}(\mathbf{b}) = 1 + i\sigma V_{\mathrm{p}0}(\mathbf{b}) + i\sigma \Delta V_{\mathrm{p}}(\mathbf{b}, t), \qquad (3)$$

where $\sigma = \pi/\lambda U_0$, $\mathbf{b} = (x, y)$, λ is the electron wavelength, U_0 is the electron acceleration voltage and V_{p} is the instantaneous crystal projected potential. Taking a Fourier transform (FT) of the wavefunction

$$\Phi(\mathbf{u}) \approx \delta(\mathbf{u}) + i\sigma \, \mathrm{FT}[V_{\mathrm{p}0}(\mathbf{b})] + i\sigma \, \mathrm{FT}[\Delta V_{\mathrm{p}}(\mathbf{b}, t)], \qquad (4)$$

where the first term represents the centre transmitted beam, the second term the Bragg reflected beams and the third term the diffusely scattered electrons. From the Abbe imaging theory, the intensity seen in the image plane is

$$I(\mathbf{b}) = \langle |[1 + i\sigma V_{\mathrm{p}0}(\mathbf{b}) + i\sigma \Delta V_{\mathrm{p}}(\mathbf{b}, t)] \otimes t_{\mathrm{obj}}(\mathbf{b})|^2 \rangle_t, \qquad (5)$$

where $\otimes$ indicates a convolution calculation, $t_{\mathrm{obj}}(x, y)$ characterizes the information transfer of the objective lens and is a Fourier transform of the objective lens transfer function $T_{\mathrm{obj}}(\mathbf{u})$, and $\langle \rangle_t$ represents the time average of the image intensity. This average is based on the 'frozen'-lattice model. This model is equivalent to the

rigorous quantum phonon excitation theory under the experimental conditions that we are interested in (Wang 1998a). With the use of $\langle \Delta V \rangle_t = 0$, the result is

$$I(\mathbf{b}) = 1 - 2\sigma V_{p0}(\mathbf{b}) \otimes \mathrm{Im}\,[t_{\mathrm{obj}}(\mathbf{b})] + \sigma^2 |V_{p0}(\mathbf{b}) \otimes t_{\mathrm{obj}}(\mathbf{b})|^2 + \sigma^2 \langle |\Delta V_p(\mathbf{b}, t) \otimes t_{\mathrm{obj}}(\mathbf{b})|^2 \rangle_t,$$
(6)

where the first term represents the incident beam, the second term the interference between the centre beam with the Bragg diffracted beams (the first-order effect), for example the bright-field lattice image, the third term is the interference between the Bragg reflected beams (the second-order effect), and the last term is the contribution made by TDS (the second-order effect). This equation clearly shows that the contribution made by TDS is the same order of magnitude as the cross-interference term between Bragg beams excluding the central transmitted beam, since ΔV is comparable with V_0 according to figure 1.

In the image contrast, the second term (the bright field term) can produce contrast reversal as the lens defocus is changed, but the intensity contributed by TDS is always the strongest at the atom sites. Therefore, at the Schertzer defocus condition under which the atomic columns are dark contrast, adding the TDS contribution can change the darkness of the atom columns, resulting in a decrease in the image contrast, possibly giving a better fit to the experimental image. This is the importance of TDS in HRTEM.

If the central transmitted beam is blocked, the dark-field HRTEM image formed by the Bragg reflected and thermal diffusely scattered electrons is

$$I_D(\mathbf{b}) = \sigma^2 |V_{p0}(\mathbf{b}) \otimes t_{\mathrm{obj}}(\mathbf{b})|^2 + \sigma^2 \langle |\Delta V_p(\mathbf{b}, t) \otimes t_{\mathrm{obj}}(\mathbf{b})|^2 \rangle_t,$$
(7)

in which about 50% of the image intensity and contrast is determined by TDS electrons!

We now examine the detailed characteristics of the image intensity contributed by TDS:

$$
\begin{aligned}
I_{\mathrm{TDS}}(\mathbf{b}) &= \sigma^2 \langle |\Delta V_p(\mathbf{b}, t) \otimes t_{\mathrm{obj}}(\mathbf{b})|^2 \rangle_t \\
&= \sigma^2 \left\langle \left| \int d\mathbf{b}' \, \Delta V_p(\mathbf{b}', t)\, t_{\mathrm{obj}}(\mathbf{b} - \mathbf{b}') \right|^2 \right\rangle_t \\
&= \sigma^2 \int d\mathbf{b}' \int d\mathbf{b}'' \langle \Delta V_p(\mathbf{b}', t) \Delta V_p(\mathbf{b}'', t) \rangle_t \, t_{\mathrm{obj}}(\mathbf{b} - \mathbf{b}')\, t_{\mathrm{obj}}^*(\mathbf{b} - \mathbf{b}''). \quad (8)
\end{aligned}
$$

The projected potential can be related to the crystal potential by

$$\langle \Delta V_p(\mathbf{b}', t) \Delta V_p(\mathbf{b}'', t) \rangle_t = \int_0^d dz_1 \int_0^d dz_2 \langle \Delta V(\mathbf{r}_1, t) \Delta V(\mathbf{r}_2, t) \rangle_t,$$
(9)

where d is the specimen thickness. The time average of the correlated perturbing potential is directly related to the mixed dynamic form factor S by a double Fourier transform (Wang 1996):

$$\langle \Delta V(\mathbf{r}', t) \Delta V(\mathbf{r}'', t) \rangle_t = \int d\mathbf{Q} \int d\mathbf{Q}' \exp\,[2\pi i (\mathbf{r}' \cdot \mathbf{Q} - \mathbf{r}'' \mathbf{Q}')]\, S(\mathbf{Q}, \mathbf{Q}'),$$
(9 a)

and for a periodic structure and in the Einstein model

$$S(\mathbf{Q}, \mathbf{Q}') = \sum_g \delta(\mathbf{Q}' - \mathbf{Q} - \mathbf{g})]F(\mathbf{Q}, \mathbf{g}), \tag{9 b}$$

where

$$F(\mathbf{Q}, \mathbf{g}) = \sum_\beta \exp\left[2\pi i r(\beta) \cdot \mathbf{g}\right] f_\beta^e(\mathbf{Q}) f_\beta^e(\mathbf{Q} + \mathbf{g}) \{\exp\left[-W_\beta(\mathbf{g})\right]$$

$$- \exp\left[-W_\beta(\mathbf{Q}) - W_\beta(\mathbf{Q} + \mathbf{g})\right]\}, \tag{9 c}$$

the sum of β is over all the atoms in the unit cell, $\mathbf{g}$ are the reciprocal-lattice vectors, the Debye–Waller factor $W_\beta(\mathbf{Q}) = 2\pi^2 \langle (\mathbf{Q} \cdot \mathbf{u}_\beta)^2 \rangle_t$, and $\mathbf{u}_\beta$ is the time-dependent displacement of the βth atom from its equilibrium position. Under the projected potential approximation, the Bragg reflections are restricted to the zero-order Laue zone, using the Fourier transform of $t_{obj}(\mathbf{b})$ and substituting of equation (9) into (8), leads to

$$I_{TDS}(\mathbf{b}) = \sigma^2 \int d\mathbf{Q} \int d\mathbf{Q}'\, S(\mathbf{Q}, \mathbf{Q}') \int_0^d dz' \int_0^d dz''\, \exp\{2\pi i[z'Q_z - z''Q_z']\}$$

$$\times \exp\{2\pi i[\mathbf{b} \cdot (\mathbf{Q}_b - \mathbf{Q}_b')]\} T_{obj}(\mathbf{Q}_b) T_{obj}^*(\mathbf{Q}_b'')$$

$$= \sigma^2 \sum_g \int d\mathbf{Q}\, F(\mathbf{Q}, \mathbf{g}) \int_0^d dz' \int_0^d dz''\, \exp\left[2\pi i(z' - z'')Q_z\right]$$

$$\times \exp\left(-2\pi i \mathbf{b} \cdot \mathbf{g}\right) T_{obj}(\mathbf{Q}_b) T_{obj}^*(\mathbf{Q}_b + \mathbf{g}). \tag{10}$$

If $F(\mathbf{Q}, \mathbf{g})$ is approximately independent of Q_z, the momentum transfer parallel to the beam direction, equation (10) is simplified to

$$I_{TDS}(\mathbf{b}) = d\sigma^2 \sum_g \exp\left(-2\pi i \mathbf{b} \cdot \mathbf{g}\right) \int d\mathbf{Q}_b\, F(\mathbf{Q}_b, \mathbf{g}) T_{obj}(\mathbf{Q}_b) T_{obj}^*(\mathbf{Q}_b + \mathbf{g}). \tag{11}$$

This equation outlines the characteristics of the TDS electron images. First, the image intensity is proportional to specimen thickness d, the first-order incoherent scattering result. Secondly, the image is a Fourier image with the periodicity of the lattice vector. This means that the image formed by the phonon-scattered electron also reflects the periodic structure of the specimen. Finally, the observed image is an incoherent summation of the images contributed by the electrons with different momentum transfers $\hbar \mathbf{Q}_b$. This incoherent integration changes only the magnitudes of the Fourier coefficients but not the image periodicity. A more rigorous treatment of the dynamic theory has been given elsewhere (Wang 1998b).

§4. SOME EXPERIMENTAL EVIDENCE

We have pointed out earlier that the energy loss of the phonon-scattered electrons is so small that they cannot be separated from the elastically scattered electrons in the image. On the other hand, they can be separated in the electron diffraction pattern because both are distributed at different angles: A uniform featureless background seen in the electron diffraction patterns, however, may not be attributed to the contribution of phonon scattering because any amorphous surface layer of the specimen can give a similar background. We must choose a material in which the vibration coupling between the atoms is so strong that the diffuse streaks are clearly produced in the diffraction pattern. Si and GaAs are excellent examples. Figure 3(a)
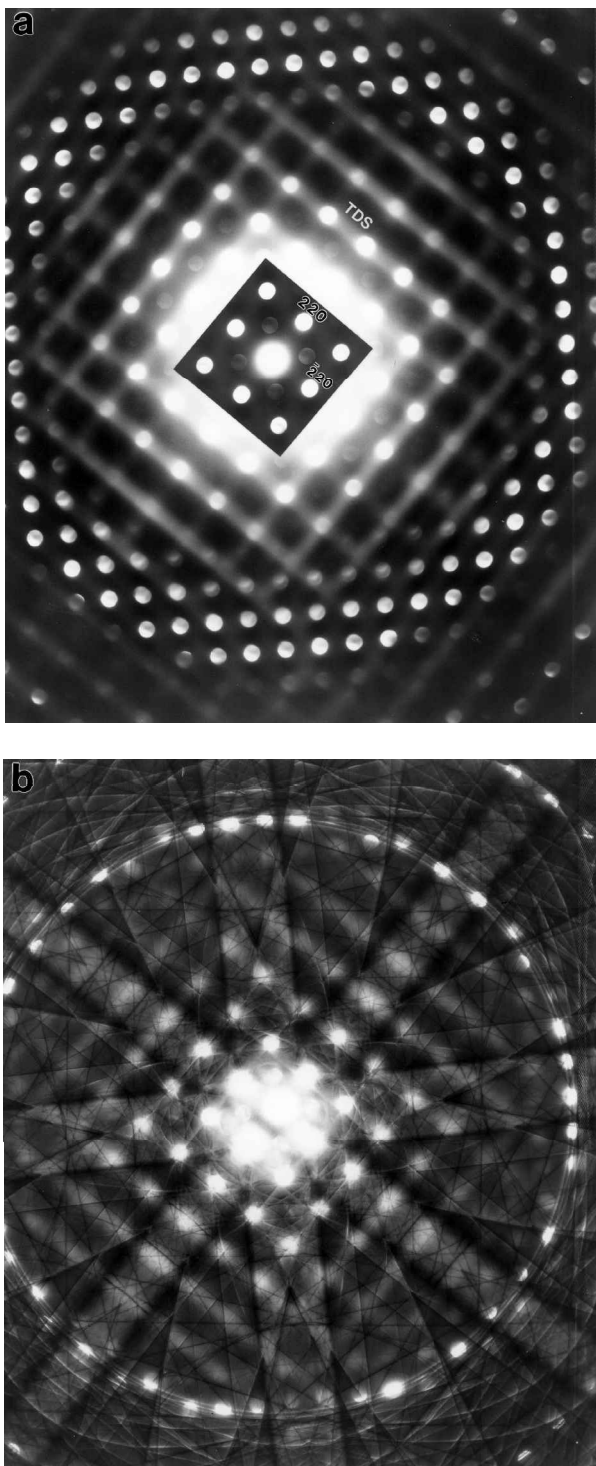
Figure 3. Experimentally observed electron diffraction patterns from (*a*) a thin and (*b*) a thick region of a GaAs foil, showing the presence of strong $\langle 110 \rangle$ TDS streaks in the pattern.

is a [100] experimental diffraction pattern recorded from a thin foil of GaAs without using an energy filter, in which clear streaks along $\langle 110 \rangle$ directions are seen (Wang 1995a). These streaks are particularly pronounced at larger scattering angles, even beyond the FOLZ, as expected theoretically (see figure 2). As the specimen thickness increases, Kikuchi lines and bands are clearly shown (figure 3(b)), and the TDS streaks are still visible except that the contrast is significantly lower. From the formation mechanism of Kikuchi patterns (Reimer 1993), the inelastic scattering processes that make appreciable contribution to the Kikuchi lines must have a large momentum transfer, or large angular spreading. To determine which of the processes are responsible for the Kikuchi pattern formation, we perform the following experiments.

In the diffraction mode, the diffraction pattern (at large camera length) can be manually scanned across the entrance aperture of the electron-energy-loss spectrometer, allowing the angle-resolved electron-energy-loss spectroscopy (EELS) of TDS electrons to be performed (Wang and Fisher 1993). The experiment was performed at 200 kV, with a camera length $L = 1.6$ m and an electron-energy-loss spectrometer of 3 mm, which gave an angular resolution of about 2 mrad. The beam convergence was controlled to the smallest to decrease the size of the Bragg spots. The energy dispersion was chosen as 0.5 eV to include a wide range of energy-losses. The EELS experiments were performed following two scanning lines, one along the (220), (440) and (660) systematic reflection row, and the other parallel to this row but half way between (000) and $(\overline{2}20)$, as labelled in figure 4(a). The zero-loss peak and the entire inelastically scattered electrons with energy-loss larger than 3 eV are integrated from the spectra, and the final result is given in figure 4(b). At the central transmitted (000) spot, the ratio $I_{(\mathrm{zero\,loss})} / I_{(\mathrm{inels})} \approx 0.95$. At the angle half-way between (000) and (220), the intensity of the elastic electrons is one sixth of the inelastically scattered electrons, while the $I_{(\mathrm{zero\,loss})} / I_{(\mathrm{inels})}$ ratio goes back to 0.62 at the (220) spot. At the angle half-way between (220) and (440), the ratio is 0.4, and at larger angles the ratio increases steadily without large fluctuation irrespective of whether the angle is at Bragg spots or TDS streaks, indicating a relative increase in the zero-loss electrons. If the contribution from the surface layer were significant, the dip observed between (000) and (220) would be absent. The measurement along line 2 gives a similar profile. To explore the distribution of the inelastically scattered electrons between (000) and (220), a finer scan was made (figure 4(c)). Despite the difference in specimen thickness used for figures 4(b) and 4(c) the $I_{(\mathrm{zero\,loss})} / I_{(\mathrm{inels})}$ ratio is a maximum at the (000) and (220) Bragg spots, while a small peak is seen at the middle.

To understand the behaviour of $I_{(\mathrm{zero\,loss})} / I_{(\mathrm{inels})}$, one needs first to examine the change in intensity of the elastically scattered electrons. It is obvious that the elastic intensity is distributed at Bragg spots; any 'elastic' intensity distributed between the Bragg spots is probably due to TDS, if the amorphous surface layer is negligible. From the theoretically calculated curve in figure 2, the TDS intensity is also small at small angles; thus, the intensity of the zero-loss peak in EELS is probably the smallest when the spectrometer is positioned half-way between (000) and (220). On the other hand, the plasmon scattering intensity is strongly centred around the central and the Bragg reflected spots and its angular spread depends on the specimen thickness. If the EELS entrance aperture is just off the (000) peak, the elastic intensity dramatically drops almost to zero, while the plasmon electron intensity is still appreciable, resulting in an extraordinary decrease in the $I_{(\mathrm{zero\,loss})} / I_{(\mathrm{inels})}$ ratio. At the larger scattering angles in figure 4(b), the $I_{(\mathrm{zero\,loss})} / I_{(\mathrm{inels})}$ ratio remains steady, either
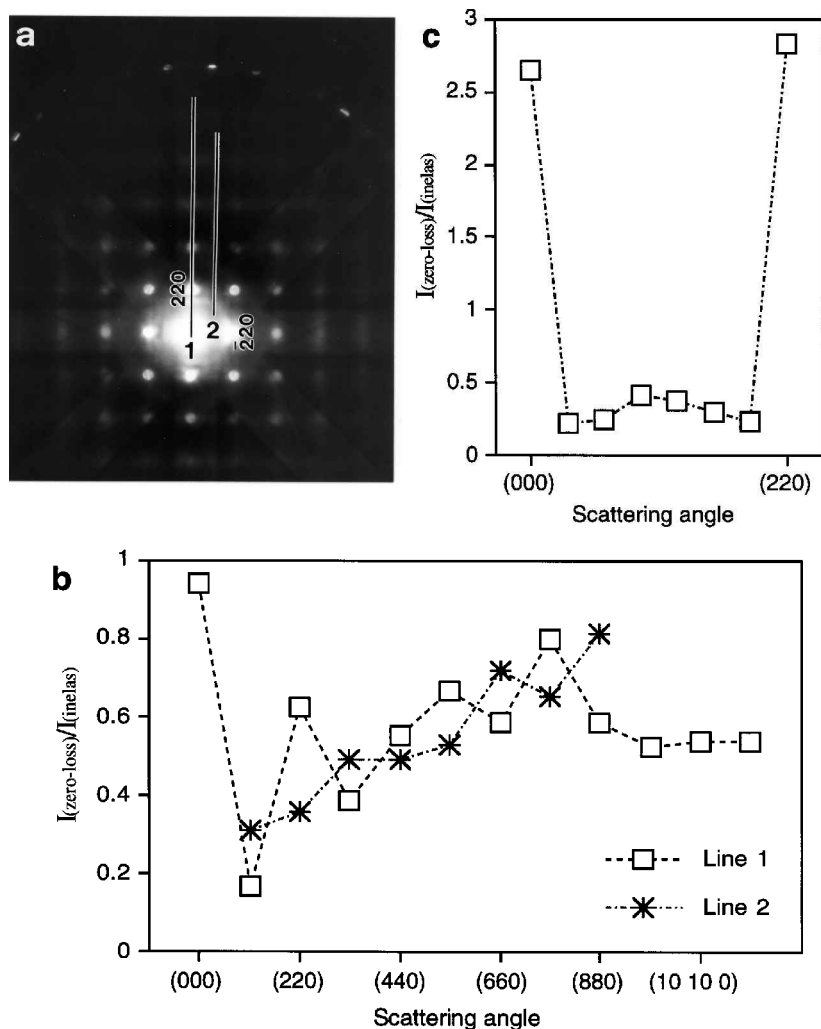
Figure 4. (*a*) An electron diffraction pattern recorded from Si[100]. (*b*) The angle-resolved intensity ratio of the total inelastically scattered electrons to the zero-loss peak measured by EELS in the diffraction mode (see text) along the lines indicated in (*a*). (*c*) The same as (*b*) except for a different region with finer scan between (000) and (220). The electron voltage is 200 kV, the camera length is 1.6 m and the EELS entrance aperture size is 3 mm.

at Bragg peaks or at TDS streaks, indicating a constant contribution of TDS electrons to the zero-loss peak, in agreement with the result of figure 2. As we pointed out, at large scattering angles, the zero-loss intensity observed between Bragg peaks can only come from TDS, and the inelastic scattering probability of the TDS electrons is determined by the specimen thickness; thus, the ratio of the TDS electrons to the inelastically scattered electrons remains to be almost a constant, for example, $I_{(zero\,loss)}/I_{(inels)}$ a constant. This result suggests the dominant contribution of TDS electrons at large angles because the elastic scattering at non-Bragg angles is expected to be zero, and their contribution to the image is analogous to the dark-field HRTEM image.
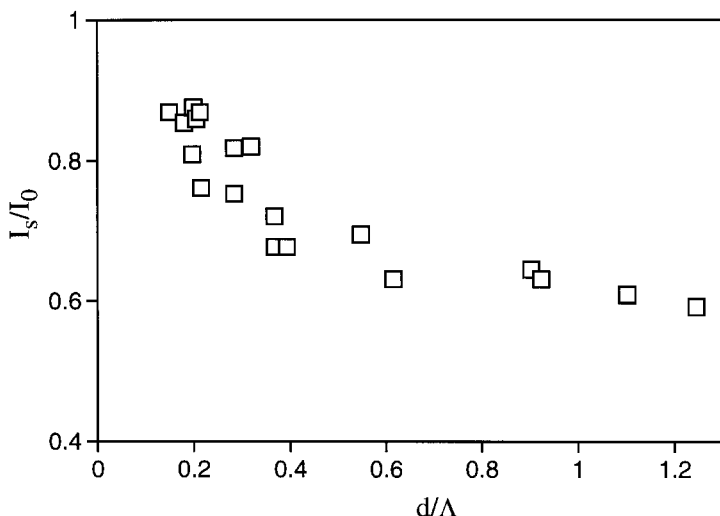
Figure 5. The ratio of the total transmission electron intensity measured by EELS in the image mode of a GaAs foil oriented along the [100] zone axis, with (I_s) and without (I_0) the presence of the specimen in the beam path, as a function of the specimen thickness d. The electron voltage 200 kV, the image magnification is $100\,000\times$ and the EELS entrance aperture size is 3 mm.

To examine the absorption effect of TDS, the total transmitted electron intensity with and without the presence of the specimen was measured. This experiment was performed using either EELS or an CCD camera as a function of the specimen thickness. To minimize the effect of beam fluctuation, a pair of electron-energy-loss spectra were acquired in the image mode, without using the objective aperture and keeping the beam illumination unchanged, with and without the specimen in the beam path. Each group of measurement took only 6 s; thus, the beam instability, if any, was negligible. The experimental result is summarized in figure 5. The horizontal axis is d/Λ, where d is the specimen thickness and Λ the inelastic mean-free-path length which is typically about 100 nm for GaAs at 200 kV. Therefore, for a specimen as thin as 15–20 nm, about 12% of the incident electrons have been lost during transmission through the specimen. Two factors may account for this loss: back scattering and scattering beyond the maximum column angle of the microscope. Both scatterings are at extremely large angles and they can only be produced by TDS. This means that, for a specimen as thin as 15–20 nm, more than 12% of the electrons have been diffusely scattered to angles larger than the maximum column angle of the transmission electron microscope (which is 15.6° in this case). These electrons together with those observed in the diffraction patterns are considered to be an absorption effect of the elastic waves. On the other hand, the TDS electrons falling inside the objective aperture can contribute to the image and they should be included in the dynamic calculation. Several theoretical approaches have been developed for this purpose (Loane *et al.* 1991, Fanidis *et al.* 1992, 1993, Dinges *et al.* 1995, Wang 1995b).

§5. CONCLUSION

With the use of an energy filter, electrons with energy losses larger than 3 eV can be removed from the image or diffraction pattern. Plasmon and the continuous

energy-loss processes (bremsstrahlung and Compton scattering) are unlikely to affect the contrast of the elastically scattered electron and thus, leave no effect on the image calculation if the specimen thickness is uniform. Atomic inner-shell excitation may not affect the image contrast because the excitation probability is extremely small. TDS is a very localized scattering process that is likely to affect the image contrast strongly. Under the weak-phase object approximation, it is shown that the contribution of the TDS electrons to the image is of the same order as the cross-interference terms for the Bragg reflected beam in the dark-field HRTEM imaging.

The distribution of the thermal diffusely scattered electrons in the diffraction plane is revealed experimentally. The result suggests the dominant effect of the thermal diffusely scattered electrons especially at large scattering angles. The TDS absorption is measured and the result indicated that about 12% of the incident electrons have been diffusely scattered to angles larger than 15.6° (the column angle of the transmission electron microscope) by a GaAs foil as thin as 15–20 nm, clearly showing the magnitude and importance of TDS in HRTEM. It is therefore mandatory to include this component in image calculation.

The conventional multislice calculation includes the Debye–Waller factor and an imaginary potential that can be tabulated or parameterized (Peng *et al.* 1996a,b). This accounts only for the effect of diffuse scattering on the Bragg reflections rather than the contribution made by TDS. An improved multislice theory or other theory including TDS must be used (Loane *et al.* 1991; Fanidis *et al.* 1992, 1993, Dinges *et al.* 1995, Wang 1995b, 1998b).

References

Coene, W. M. J., Janssen, A. J. E. M., Denteneer, T. J. J., Op De Beeck, M., and Van Dyck, D., 1994, *Microsc. Soc. Am. Bull.,* **24**, 472.

Cowley, J. M., 1988, *Acta crystallogr.* A, **44**, 847.

Dehm, G., Ernst, F., Mayer, J., Möbus, G., Müllejans, Phillipp, F., Scheu, C., and Rühle, M., 1996, *Z. Metallk.,* **87**, 898.

Dinges, C., Berger, A., and Rose, H., 1995, *Ultramicroscopy,* **60**, 49.

Egerton, R. F. 1996, *Electron Energy Loss Spectroscopy in the Electron Microscope,* second edition (New York: Plenum).

Fanidis, C., Van Dyck, D., and Landuyt, J. 1992, *Ultramicroscopy,* **41**, 55; 1993, *Ultramicroscopy,* **48**, 133.

Hall, C. R., and Hirsch, P. B., 1965, *Proc. R. Soc.* A, **286**, 158.

Loane, R. F., Xu, P., and Silcox, J., 1991, *Acta crystallogr.* A, **47**, 267.

Peng, L. M., Ren, G., Dudarev, S. L., and Whelan, M. J., 1996a, *Acta crystallogr.* A, **52**, 456; 1996b, *Acta crystallogr.* A, **52**, 257.

Reimer, L., 1993, *Transmission Electron Microscopy* (New York: Springer).

Rossouw, C. J., Miller, P. R., Drennan, J., and Allen, L. J., 1990, *Ultramicroscopy* **34**, 149.

Van Dyck, D., 1997 (to be published).

Van Dyck, D., Lichte, H., and van der Mast, K. D., 1997, *Ultramicroscopy,* **64**, 1.

Wang, Z. L., 1995a, *Elastic and Inelastic Scattering in Electron Diffraction and Imaging* (New York: Plenum); 1995b, *Acta crystallogr.* A, **51**, 569; 1996, *ibid.,* **52**, 717; 1998a, *ibid.,* **54**, 460; 1998b, *Ultramicroscopy* (to be published).

Wang, Z. I., and Fisher, A. T., 1993, *Ultramicroscopy,* **48**, 183.